A&A 653, A90 (2021)
https://doi.org/10.1051/0004-6361/202140979

Astronomy & Astrophysics

Exploiting the *Gaia* EDR3 photometry to derive stellar temperatures

A. Mucciarelli[1,2], M. Bellazzini[2], and D. Massari[2,3]

[1] Dipartimento di Fisica e Astronomia Augusto Righi, Università degli Studi di Bologna, Via Gobetti 93/2, 40129 Bologna, Italy
e-mail: alessio.mucciarelli2@unibo.it
[2] INAF – Osservatorio di Astrofisica e Scienza dello Spazio di Bologna, Via Gobetti 93/3, 40129 Bologna, Italy
[3] University of Groningen, Kapteyn Astronomical Institute, 9747 AD Groningen, The Netherlands

Received 1 April 2021 / Accepted 3 June 2021

ABSTRACT

We present new colour–effective temperature ($T_{\rm eff}$) transformations based on the photometry of the early third data release (EDR3) of the ESA/*Gaia* mission. These relations are calibrated on a sample of about 600 dwarf and giant stars for which $T_{\rm eff}$ has previously been determined with the infrared flux method from dereddened colours. The 1σ dispersion of the transformations is of 60–80 K for the pure *Gaia* colours $(BP-RP)_0$, $(BP-G)_0$, and $(G-RP)_0$, improving to 40–60 K for colours including the 2MASS K_s-band, namely $(BP\text{-}K_s)_0$, $(RP-K_s)_0$, and $(G-K_s)_0$. We validate these relations in the most challenging case of dense stellar fields, where the *Gaia* EDR3 photometry could be less reliable, providing guidance for the safe use of *Gaia* colours in crowded environments. We compare the $T_{\rm eff}$ from the *Gaia* EDR3 colours with those obtained from standard $(V-K_s)_0$ colours for stars in three Galactic globular clusters of different metallicity, namely NGC 104, NGC 6752, and NGC 7099. The agreement between the two estimates of $T_{\rm eff}$ is excellent, with mean differences of between –50 and +50 K, depending on the colour, and with 1σ dispersions around the mean $T_{\rm eff}$ differences of 25–50 K for most of the colours and below 10 K for $(BP-K_s)_0$ and $(G-K_s)_0$. This demonstrates that these colours are analogous to $(V-K_s)_0$ as $T_{\rm eff}$ indicators.

Key words. stars: fundamental parameters – stars: atmospheres – techniques: photometric

1. Introduction

Effective temperatures ($T_{\rm eff}$) for FGK-spectral type stars can be estimated with different methods either based directly on the stellar spectra, for example the wings of the Balmer lines, the line–depth ratio, and the excitation equilibrium, or on the photometric properties. The infrared flux method (IRFM, Blackwell & Shallis 1977; Blackwell et al. 1979, 1980) is one of the most popular methods based on photometric colours, requiring accurate and precise photometry (especially for the infrared spectral range) and knowledge of the colour excess, $E(B-V)$. Several implementations of this method have been presented in the literature (see e.g. Alonso et al. 1999; Ramírez & Meléndez 2005; González Hernández & Bonifacio 2009; Casagrande et al. 2010). $T_{\rm eff}$ derived with this method for suitable calibrators is also used to obtain relations between different broad-band colours and $T_{\rm eff}$, enabling an immediate estimate of $T_{\rm eff}$ even for stars for which the IRFM cannot be directly used.

The ESA/*Gaia* mission (Gaia Collaboration 2016) is providing accurate and precise all-sky photometry in three broad-band photometric filters, named G, BP, and RP. *Gaia* DR2 colour–$T_{\rm eff}$ transformations calibrated on IRFM $T_{\rm eff}$ have been presented by Mucciarelli & Bellazzini (2020, MB20 hereafter) and Casagrande et al. (2021).

The recent *Gaia* Early Data Release 3 (EDR3, Gaia Collaboration 2021) has significantly improved upon the previous DR2, including astrometric and photometric information for about 1.5 billion stars. The superior quality of *Gaia* EDR3 photometry and its internal homogeneity (Yang et al. 2021; Riello et al. 2020, R20 hereafter) guarantees further improvement in the determination of stellar parameters. In this paper we present new colour–$T_{\rm eff}$ transformations based on *Gaia* EDR3 and 2MASS photometry, validating these relations in the case of crowded stellar fields.

2. New colours–$T_{\rm eff}$ transformations

Following the same procedure adopted in MB20, we derived colour–$T_{\rm eff}$ transformations for different broad-band colours including the *Gaia* passbands. We used the IRFM $T_{\rm eff}$ computed by González Hernández & Bonifacio (2009) for a sample of about 450 dwarf stars ($\log g > 3.0$) and about 200 giant stars ($\log g < 3.0$) with metallicity between [Fe/H] ~ -4.0 and 0.0 dex. The broad-band colours that we considered in the analysis are $(BP-RP)_0$, $(BP-G)_0$, $(G-RP)_0$, $(G-K_s)_0$, $(BP-K_s)_0$ and $(RP-K_s)_0$. These were derived adopting the *Gaia* EDR3 photometry (Gaia Collaboration 2021) and the K_s-band magnitudes from the Two Micron All Sky Survey (2MASS, Skrutskie et al. 2006). *Gaia* magnitudes have been corrected for interstellar reddening following the iterative procedure described in Gaia Collaboration (2018), while K_s magnitudes have been corrected adopting the extinction coefficient by McCall (2004). Colour excess values $E(B-V)$ are the same as those used by González Hernández & Bonifacio (2009).

We computed the best polynomial fit relating each colour C with θ (defined as $\theta = 5040/T_{\rm eff}$) and the stellar metallicity [Fe/H], according to the functional form:

$$\theta = b_0 + b_1 C + b_2 C^2 + b_3[\mathrm{Fe/H}] + b_4[\mathrm{Fe/H}]^2 + b_5[\mathrm{Fe/H}]C, \quad (1)$$

Table 1. Coefficients b_0,...,b_5 of the colour–$T_{\rm eff}$ relations.

Colour	Colour range (mag)	$\sigma_{T_{\rm eff}}$ (K)	N	b_0	b_1	b_2	b_3	b_4	b_5
Dwarf stars									
$(BP - RP)_0$	[0.39–1.50]	61	436	0.4929	0.5092	–0.0353	0.0192	–0.0020	–0.0395
$(BP - G)_0$	[0.13–0.69]	58	418	0.5316	1.2452	–0.4677	0.0068	–0.0031	–0.0752
$(G - RP)_0$	[0.25–0.81]	62	439	0.5050	0.6532	0.2284	0.0260	–0.0011	–0.0726
$(BP - K_s)_0$	[0.62–3.21]	44	439	0.5342	0.2044	–0.0021	0.0276	0.0005	–0.0158
$(RP - K_s)_0$	[0.34–1.74]	53	435	0.5526	0.3712	–0.0121	0.0330	0.0029	–0.0220
$(G - K_s)_0$	[0.53–2.54]	48	443	0.5351	0.2440	0.0016	0.0289	0.0015	–0.0163
Giant stars									
$(BP - RP)_0$	[0.33–1.81]	83	209	0.5323	0.4775	–0.0344	–0.0110	–0.0020	–0.0009
$(BP - G)_0$	[0.11–0.89]	83	208	0.5701	1.1188	–0.3710	–0.0236	–0.0039	0.0070
$(G - RP)_0$	[0.22–0.92]	71	201	0.5472	0.5914	0.2347	–0.0119	–0.0012	0.0060
$(BP - K_s)_0$	[0.68–3.97]	49	211	0.5668	0.1890	–0.0017	0.0065	–0.0008	–0.0045
$(RP - K_s)_0$	[0.35–2.23]	61	215	0.5774	0.3637	–0.0226	0.0346	0.0007	–0.0221
$(G - K_s)_0$	[0.57–3.10]	46	206	0.5569	0.2436	–0.0035	0.0211	0.0007	–0.0089

Notes. For each relation are listed also the corresponding colour range, the dispersion of the fit residuals, and the number of stars used.

and considering dwarf and giant stars separately. A few outliers have been removed adopting an iterative 2.5σ-clipping procedure. Table 1 lists the colour range of validity, the number of stars used for the fit, the 1σ dispersion of the fit residuals, and the coefficients $b_0, \ldots, b_5$, for both dwarf and giant stars samples.

The colour–$T_{\rm eff}$ relations that we obtained in this way have typical 1σ dispersion of ~40–60 K and ~40–80 K, for dwarf and giant stars, respectively. The 1σ dispersion of the relations is usually adopted as a conservative estimate of the uncertainty in the derived $T_{\rm eff}$ when this kind of colour–$T_{\rm eff}$ relation is provided and/or used (see e.g. Alonso et al. 1999; González Hernández & Bonifacio 2009; Casagrande et al. 2021). This uncertainty should be added in quadrature to that obtained by propagating the error on colour. The uncertainty in [Fe/H] has a negligible impact on the derived $T_{\rm eff}$, as a variation of ±0.1 dex leads to a change in $T_{\rm eff}$ of smaller than ~10 K, depending on the adopted relation. Finally, we verified that the temperature differences given by the relations for dwarfs and giants at the adopted dwarf–giant threshold (log g = 3.0) is about 10–20 K, significantly smaller than the uncertainties.

In the common practice of abundance analysis, a full propagation of the errors, including errors in the relation coefficients, is not adopted (we are not aware of a single example in the literature for the field of stellar population studies). The uncertainties involved in the whole process of abundance estimates are so many and so deeply entangled that a full propagation can be prone to underestimation of the actual errors on the abundances. However, for application cases requiring full error propagation on the final $T_{\rm eff}$ estimates, in Appendix B we provide (a) alternative relations adopting differences with respect to the mean colour as an independent variable (e.g. using $(BP - RP)_0$ $\langle(BP - RP)_0\rangle$, instead of $(BP - RP)_0$ alone) to minimise the off-diagonal terms of the covariance matrix, and (b) the full covariance matrices for all the relations.

The new transformations are very similar to those provided by MB20 based on *Gaia* DR2 photometry, reflecting the similarity between the DR2 and EDR3 photometric systems. The use of the old relations with *Gaia* EDR3 photometry provides $T_{\rm eff}$ that differ by less than 40–50 K from those obtained with the new relations. Also, the new transformations have 1σ dispersion similar to or smaller than those obtained with DR2 photometry. In particular, we noted that the dispersions of all of the transformations including the G-band magnitudes are reduced by ~20–30% with respect to those obtained with *Gaia* DR2 photometry. Indeed, according to R20, the most significant improvements between DR2 and EDR3 photometry occurred in the bright star regime that is spanned by our calibrating sources (G < 6.0).

Figures A.1–A.6 show the colour–$T_{\rm eff}$ trends for the adopted calibrating sample and the corresponding polynomial fit. The stars are coloured according to the metallicity interval they belong to: [Fe/H] ≤ −2.5 dex (blue points),−2.5 < [Fe/H] ≤ −1.5 (green points), −1.5 < [Fe/H] ≤ −0.5 (red points), [Fe/H] > −0.5 dex (black points). Finally, Fig. A.7 shows the behaviour of the fit residuals as a function of [Fe/H] for all the relations.

We compared the predictions of the Casagrande et al. (2021) relations with ours for the stars of our calibrating sample, using all the colours that can be obtained by combining the three *Gaia* pass-bands and then also combining these with 2MASS K. The mean differences are within ≃±100 K and the scatter is small (spanning ≲50 K) in all cases except for the $(BP - G)_0$ colour, where dwarfs display a mean difference of about 250 K and a significant scatter (≳100 K). Taking into account that part of the observed differences may be due to the subtle changes between *Gaia* DR2 and EDR3 photometry (especially for G ≤ 13.0, see Evans et al. 2018, R20), we can conclude that the two calibrations provide consistent results within the uncertainties. The Casagrande et al. (2021) relations use 14 coefficients and explicitly include the dependency on surface gravity; they may therefore be appropriate when all the astrophysical parameters of the target stars, except $T_{\rm eff}$, are already known with high accuracy. On the other hand, our relations account for the very small effect of surface gravity by means of a simple giant–dwarf dichotomy and are defined by just five parameters; they are simpler and have a wider range of applicability in most real cases.

3. Application on three globular clusters: NGC 104, NGC 6752, M 30

The new relations are based on isolated bright field stars for which *Gaia* provides superb photometry that is usually not affected by issues related to stellar contamination and/or background subtraction. To test the effectiveness of our relations in determining reliable $T_{\rm eff}$ in any condition, we decided to validate them in dense stellar fields, where the superior photometric quality of the *Gaia* magnitudes can be hampered by the high stellar crowding.

The selected stellar fields with which we perform such a test correspond to three Galactic globular clusters (GCs), namely NGC 104 (47 Tucanae), NGC 6752, and NGC 7099 (M 30). These were selected according to the following criteria:

1. They must span the entire range of metallicity covered by the population of Galactic clusters, with the selection of a metal-rich GC [NGC 104, [Fe/H] = –0.75 dex), a metal-intermediate GC (NGC 6752, [Fe/H] = –1.49 dex), and a metal-poor GC (NGC 7099, [Fe/H] = –2.31 dex) according to the iron abundances derived by Mucciarelli & Bonifacio (2020). The reason behind the choice of clusters with different [Fe/H] is to check the validity of our transformations against the metallicity, because this parameter enters our Eq. (1) directly;

2. They must have a low colour excess $E(B-V)$ (between 0.04 and 0.07 mag, see Mucciarelli & Bonifacio 2020) in order to minimise the effect of uncertainties in the extinction on the derivation of $T_{\rm eff}$;

3. They must have available ground-based V photometry from the database maintained by P. B. Stetson (Stetson et al. 2019) and $K_{\rm s}$-band photometry from 2MASS Skrutskie et al. (2006). This is to derive a reference $T_{\rm eff}$ using homogeneous $(V-K_{\rm s})_0$ colours.

Clusters members were first selected to have proper motions within 1.5 mas yr^{-1} (for NGC 104 and NGC 6752) and 1.0 mas yr^{-1} (for NGC 7099) from the cluster mean proper motions as given by Baumgardt et al. (2019). Then we filtered stars based on 'goodness of measure' EDR3 quality parameters, following prescriptions provided by Lindegren et al. (2018) and R20, including in our final samples only stars with: *(i)* ruwe < 1.4; and *(ii)* $|C^*| < 2\sigma_{\rm c}$, where C^* and $\sigma_{\rm c}$ are defined according to Eq. (6) and (18), respectively, in R20.

For these cluster stars we computed $T_{\rm eff}$ adopting the six colour–$T_{\rm eff}$ transformations derived in Sect. 2. Additionally, reference $T_{\rm eff}$ were computed using the $(V-K_{\rm s})_0$-$T_{\rm eff}$ transformation by González Hernández & Bonifacio (2009). The latter is based on the same sample of stars and IRFM $T_{\rm eff}$ used to derived our own relations, and therefore all these $T_{\rm eff}$ are on the same scale. We restricted this analysis to the stars with $G < 17$ and with error in $(V-K_{\rm s})_0$ smaller than 0.03 mag in order to exclude stars with large uncertainties in the 2MASS $K_{\rm s}$ magnitudes. To be sure that the different fitting procedures used here for the *Gaia* colours and used by González Hernández & Bonifacio (2009) for $(V-K_{\rm s})_0$ do not introduce systematic errors in the computed $T_{\rm eff}$, we derived the $(V-K_{\rm s})_0$-$T_{\rm eff}$ transformation adopting our procedure and the $(V-K_{\rm s})_0$ already used by González Hernández & Bonifacio (2009). The average difference in the $T_{\rm eff}$ from the two $(V-K_{\rm s})_0$-$T_{\rm eff}$ transformations for the cluster stars is of +1 K (σ = 6 K). Hence, our fitting procedure does not introduce differences with respect to the transformations by González Hernández & Bonifacio (2009) and we can compare $T_{\rm eff}$ from *Gaia* and $(V-K_{\rm s})_0$ colours.

From the results of our analysis, it is clear that there are advantages and disadvantages to using each of the photometric colours as a $T_{\rm eff}$ indicator, because of the different wavelength baseline and their sensitivity to $T_{\rm eff}$, and other parameters, such as metallicity and surface gravity. Here we adopt $T_{\rm eff}$ from the $(V-K_{\rm s})_0$ colour as reference values to check the robustness of those derived from *Gaia* EDR3 photometry. The $(V-K_{\rm s})_0$ colour is one of the most common and reliable photometric indicators of $T_{\rm eff}$ (see e.g. Fernley 1989; Bessell et al. 1998; Alonso et al. 1999) because of two main factors:
(i) the different sensitivity to $T_{\rm eff}$ of the flux in V- and $K_{\rm s}$-bands. This effect is clearly visible in Fig. 1, which shows a set of synthetic fluxes with $T_{\rm eff}$ from 4000 to 6000 K in steps of 250 K. All the synthetic spectra have been calculated with the SYNTHE spectral synthesis code (Kurucz 2005). The V-band flux is highly sensitive to $T_{\rm eff}$, increasing by a factor of ten as $T_{\rm eff}$ ranges from 4000 to 6000 K. On the other hand, the $K_{\rm s}$-band flux increases by only a factor of 1.5 in spite of the same $T_{\rm eff}$ change. Therefore, $(V-K_{\rm s})_0$ effectively behaves as the ratio between a $T_{\rm eff}$-sensitive flux and an almost $T_{\rm eff}$-insensitive flux.
(ii) The Johnson–Cousins V band photometry is better standardised than other optical bands, for example the B and I bands, whose definitions can vary depending on the adopted photometric system (Bessell & Brett 1988).

Figure 2 shows the behaviour of the differences between $T_{\rm eff}$ from *Gaia* EDR3 colours and from $(V-K_{\rm s})_0$ as a function of the latter for the stars in the three GCs. The average values of these differences, the corresponding 1σ dispersion, and number of stars are listed in Table 2.

$T_{\rm eff}$ from pure *Gaia* EDR3 colours have mean differences with respect to the reference $T_{\rm eff}$ of between +20 and +50 K, with scatter between 25 and 50 K. In the case of the metal-rich GC NGC 104 a mild trend of $\Delta T_{\rm eff}$ with the reference $T_{\rm eff}$ exists, in the sense that the *Gaia* EDR3 $T_{\rm eff}$ becomes slightly hotter than those from $(V-K_{\rm s})_0$ for the coldest stars.

The colours including $K_{\rm s}$ magnitudes show small average differences and 1σ dispersions; in particular, $(BP-K_{\rm s})_0$ and $(G-K_{\rm s})_0$ provide the best agreement with the $T_{\rm eff}$ from $(V-K_{\rm s})_0$, with 1σ dispersions smaller than 10 K. This simple test demonstrates that:

– (*Gaia*-$K_{\rm s}$) colours are analogous to $(V-K_{\rm s})_0$ as $T_{\rm eff}$ indicators because they have a large wavelength baseline including filters with different sensitivity in $T_{\rm eff}$;

– the calibrations based on field (isolated) stars also work well in crowding conditions typical of nearby Galactic GCs ($D \lesssim$ 10.0 kpc) once the simple selections based on quality parameters described above are adopted (see below, for further discussion).

4. How to derive accurate $T_{\rm eff}$ in crowded stellar fields

The use of the *Gaia* EDR3 photometry to infer $T_{\rm eff}$ in dense stellar fields (like globular clusters) needs a note of caution because the *Gaia* magnitudes, regardless of their formal small uncertainties, can be affected by issues concerning the background subtraction and contamination by neighbouring stars (R20).

The left panels of Fig. 3 show the three colour–magnitude diagrams for NGC 104 including pure *Gaia* colours. At variance with $(BP-RP)_0$, the other two colours show an asymmetric broadening of the red giant branch (RGB) that becomes more evident for $G > 14$. In particular, an excess of stars bluer than the main locus of the RGB is visible when we use $(BP-G)_0$, while with $(G-RP)_0$ the situation is the opposite, with an excess of redder stars. These anomalous colours translate to anomalous $T_{\rm eff}$ that can be as discrepant as ±500 K compared to RGB stars

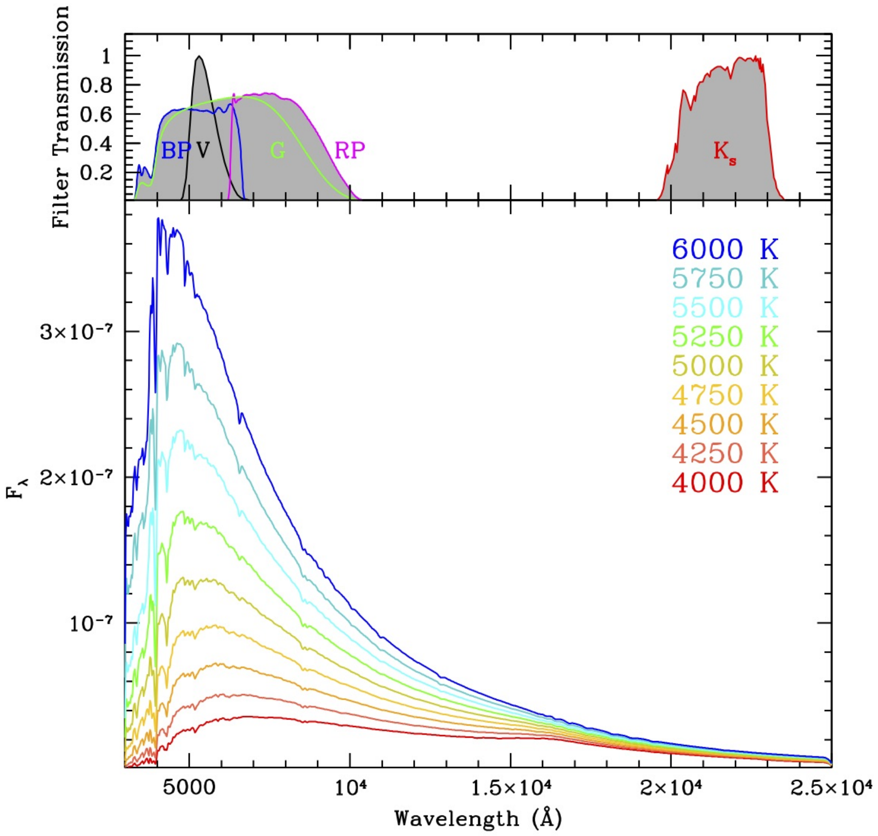

Fig. 1. *Main panel:* synthetic spectra calculated with $T_{\rm eff}$ from 4000 K (spectrum with the lower flux) to 6000 K (spectrum with the higher flux) in steps of 250 K. All the spectra adopt [M/H] = –1.0 dex. The *upper panel* shows the profile of the photometric filters used in this work.

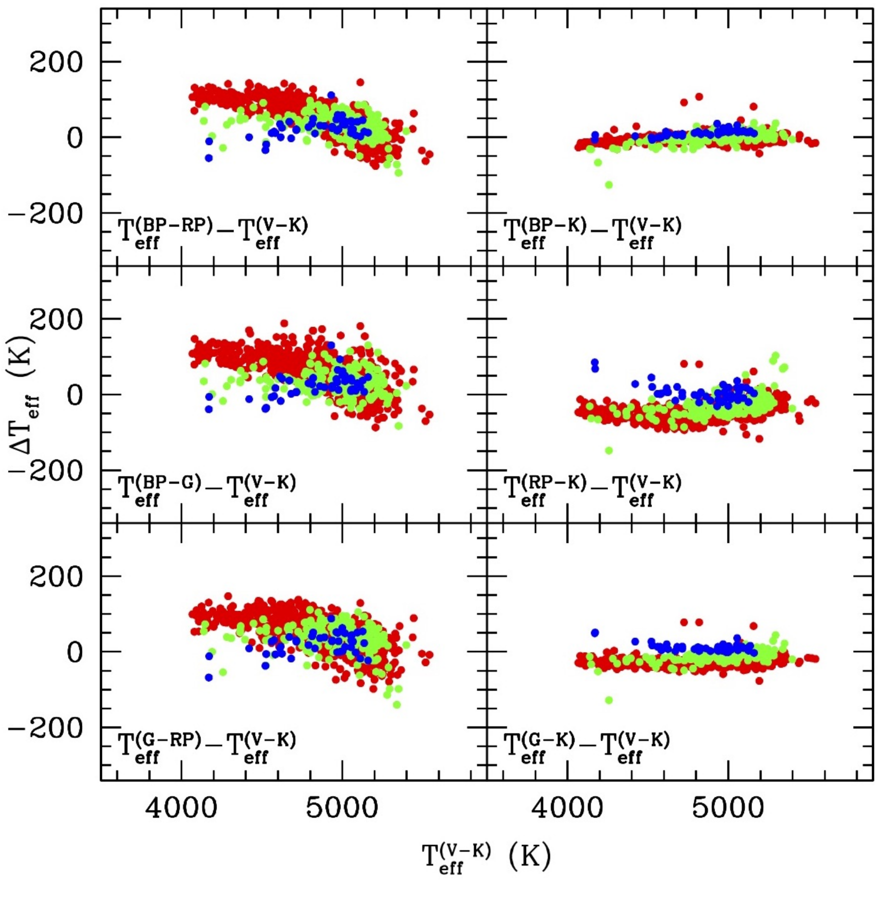

Fig. 2. Differences between $T_{\rm eff}$ derived from the *Gaia* colours and from $(V - K_s)_0$ as a function of the $(V - K_s)_0$based $T_{\rm eff}$ for the giant stars in three Galactic GCs, namely NGC 7099 (blue points), NGC 6752 (green points), and NGC 104 (red points).

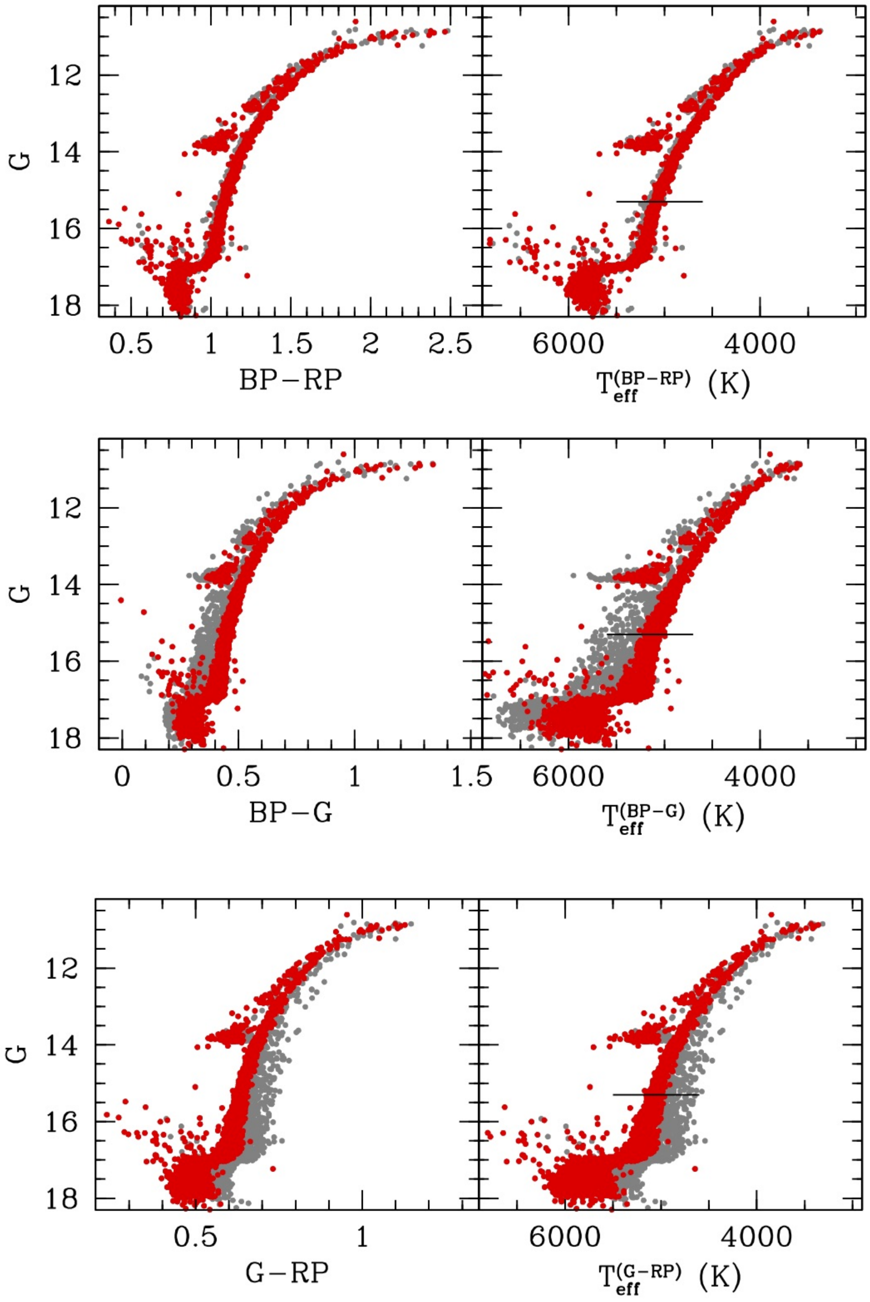

Fig. 3. Colour-magnitude diagrams for NGC 104 considering the pure *Gaia* colours (*left panels*) and the corresponding $T_{\rm eff}$ vs. *G*-band magnitudes diagrams (*right panels*). Red and grey points mark the stars selected and rejected according to the criterion provided by R20, respectively. The horizontal lines in the right panels mark the transition between the dwarf and giant star regimes.

with the same *G* magnitude. Indeed, BP and RP magnitudes are known to be more prone than *G* magnitudes to contamination from light not related to the target sources (e.g. nearby stars), for reasons inherent to the different way in which BP/RP and G fluxes are acquired and processed (R20).

Stars with anomalous colours can be easily identified and excluded by applying the criterion used in Sect. 2 for the three target clusters ($| C^* | < 2\sigma_{\rm c}$). In Fig. 3 the sources fulfilling this criterion (therefore considered as high-quality/reliable photometry sources) are shown as red circles, while those excluded are shown as grey circles. This exercise provides three important results. (i) The criterion $| C^* | < 2\sigma_{\rm c}$ allows us to efficiently identify stars with possible issues related to background subtraction and stellar contamination; (ii) Furthermore, this procedure is essential whether $(BP - G)_0$ or $(G - RP)_0$ are used; only reliable sources provide reliable $T_{\rm eff}$ while the other sources significantly over- or under-estimate (for $(G - RP)_0$ and $(BP - G)_0$, respectively) $T_{\rm eff}$. (iii) Lastly the symmetrical effect observed in $(G - RP)_0$ and $(BP - G)_0$ (and in the corresponding $T_{\rm eff}$) is largely cancelled out when $(BP - RP)_0$ is adopted. Indeed, $(BP - RP)_0$ of reliable and contaminated stars provide indistinguishable $T_{\rm eff}$.

In conclusion, according to this limited set of experiments, reliable $T_{\rm eff}$ in (non-extreme) crowded fields can be obtained by removing stars with corrupted colours with criteria based on quality parameters provided in the *Gaia* source catalogue. The criterion proposed here ($| C^* | < 2\sigma_{\rm c}$) is simple and very effective in the considered cases, but there may be cases where only stars not fulfilling such criteria are available for the analysis. The results presented above suggest that reliable $T_{\rm eff}$ estimates can also obtained for these stars using $(BP - RP)_0$ as $T_{\rm eff}$ an indicator, and taking advantage of the fact that BP and RP magnitudes are similarly affected by any light contamination entering the

Table 2. Average differences between $T_{\rm eff}$ derived from the *Gaia* EDR3 colours and $(V-K_s)_0$ for the globular clusters NGC 104, NGC 6752, and NGC 7099.

$\Delta T_{\rm eff}$	NGC 104			NGC 6752			NGC 7099		
	$\langle\Delta T_{\rm eff}\rangle$	σ	$N_{\rm star}$	$\langle\Delta T_{\rm eff}\rangle$	σ	$N_{\rm star}$	$\langle\Delta T_{\rm eff}\rangle$	σ	$N_{\rm star}$
	(K)	(K)		(K)	(K)		(K)	(K)	
$(BP-RP)_0-(V-K_s)_0$	+48	45	699	+35	26	185	+24	18	41
$(BP-G)_0-(V-K_s)_0$	+54	48	697	+31	28	185	+19	25	42
$(G-RP)_0-(V-K_s)_0$	+51	41	685	+41	24	178	+20	24	42
$(BP-K_s)_0-(V-K_s)_0$	–3	7	671	+2	8	171	+11	8	43
$(RP-K_s)_0-(V-K_s)_0$	–45	19	686	–31	15	178	+0	15	41
$(G-K_s)_0-(V-K_s)_0$	–25	8	684	–10	9	179	+9	7	41

Notes. The 1σ dispersion and the number of stars used are listed.

aperture window of BP and RP spectrophotometry (see R20, for a discussion on this subject).

5. The impact of the *Gaia* $T_{\rm eff}$ on the chemical abundances

As a sanity check, we evaluated the impact of the new colour–$T_{\rm eff}$ transformations derived from *Gaia* EDR3 photometry on the chemical abundances from high-resolution spectra. We consider the data set of high-resolution spectra acquired with the spectrograph UVES at the Very Large telescope of ESO for giant stars in 16 Galactic GCs already analysed by Mucciarelli & Bonifacio (2020). The iron abundance of these stars were derived following the same procedure adopted by Mucciarelli & Bonifacio (2020) and using the new $T_{\rm eff}$ scales. These new [Fe/H] values were compared with those obtained for the same stars from $(V-K_s)_0$ by Mucciarelli & Bonifacio (2020).

In the case of pure *Gaia* colours, the new $T_{\rm eff}$ are comparable with those from $(V-K_s)_0$, with differences smaller than 100 K. These new $T_{\rm eff}$ lead to higher [Fe/H], with differences of between 0.01 and 0.05 dex with respect to the values obtained from $(V-K_s)_0$ $T_{\rm eff}$. Figure 4 shows, as an example, the difference in the derived [Fe/H] when adopting $T_{\rm eff}$ from $(BP-RP)_0$ or $(V-K_s)_0$. The average [Fe/H] difference is +0.03 dex ($\sigma=$ 0.01 dex). The *Gaia* colours including K_s magnitudes provide a value of $T_{\rm eff}$ for the spectroscopic targets that is almost indistinguishable from the one from $(V-K_s)_0$, such that the average impact in terms of [Fe/H] is smaller than 0.01 dex. We conclude that the use of $T_{\rm eff}$ from *Gaia* EDR3 photometry leads to chemical abundances that are fully consistent with those obtained adopting $T_{\rm eff}$ from standard colours.

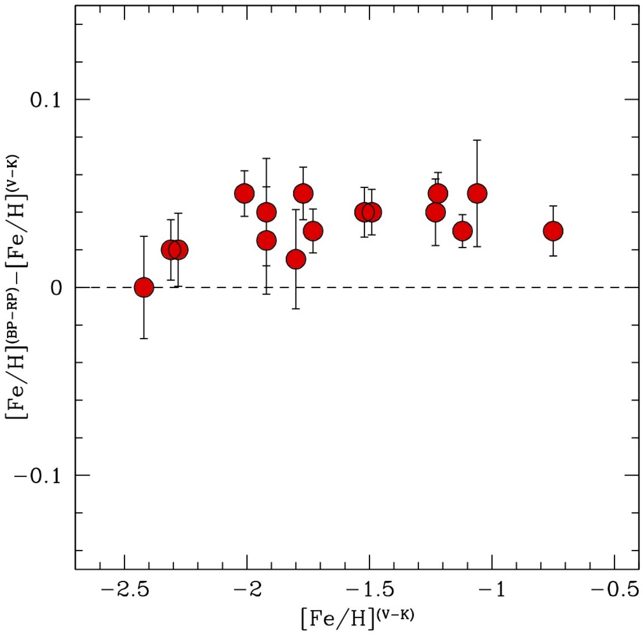

Fig. 4. Behaviour of $(V-K_s)_0$- and $(BP-RP)_0$-based [Fe/H] as a function of the iron content [Fe/H] derived from $(V-K_s)_0$-based $T_{\rm eff}$ for the 16 Galactic GCs analysed by Mucciarelli & Bonifacio (2020).

6. Conclusions

We exploited the *Gaia* EDR3 photometry to derive new colour–$T_{\rm eff}$ transformations based on the IRFM $T_{\rm eff}$ provided by González Hernández & Bonifacio (2009) for a sample of about 600 bright dwarf and giant field stars. These transformations have typical uncertainties of 40–80 K and 40–60 K for giant and dwarf stars, respectively. We checked the validity of these transformations in the case of GC stars, where the superior photometric quality of the *Gaia* magnitudes can be hampered by the high stellar crowding, providing guidelines for safe estimates of $T_{\rm eff}$ in these cases. In summary, the *Gaia* EDR3 photometry can be safely used to derive precise and accurate $T_{\rm eff}$ with the following recommendations:

1. When reliable K_s-band photometry is available, mixed colours (*Gaia*–K_s) should be preferred, as they display the maximum sensitivity to temperature. In particular, $(BP-K_s)_0$ and $(G-K_s)_0$ are the best choices because their colour–$T_{\rm eff}$ transformation shows the smallest dispersion and the best agreement with $T_{\rm eff}$ derived from $(V-K_s)_0$;
2. When K_s-band photometry is not available or is not sufficiently precise, pure *Gaia* colours can be used to derive $T_{\rm eff}$, although they show slightly larger dispersion with respect to the broad band colours including K_s;
3. BP- and RP-band magnitudes in crowded fields can be affected by issues concerning stellar blending and background subtraction, despite their high photometric precision. For this reason, $(G-RP)_0$ and $(BP-G)_0$ can lead to under- and over-estimated $T_{\rm eff}$, respectively. To avoid these effects, stars should be selected according to C^* and we recommend the criterion $|C^*|<2\sigma_c$. Alternatively, $(BP-RP)_0$ should be preferred over other combinations of *Gaia* magnitudes,

because the effects of contamination from light not related to the target source are similar in the BP and RP bands and almost cancel out when subtracted.

Acknowledgements. We thank the referee, Floor van Leeuwen, for the comments and suggestions that improved the manuscript. We also thank Paolo Montegriffo for the useful discussions. This work has made use of data from the European Space Agency (ESA) mission *Gaia* (`https://www.cosmos.esa.int/gaia`), processed by the *Gaia* Data Processing and Analysis Consortium (DPAC, `https://www.cosmos.esa.int/web/gaia/dpac/consortium`). Funding for the DPAC has been provided by national institutions, in particular the institutions participating in the *Gaia* Multilateral Agreement. This research has made extensive use of the R programming language and R Studio environment.

References

Alonso, A., Arribas, S., & Martinez-Roger, C. 1999 A&AS, 140, 261
Baumgardt, H., Hilker, M., Sollima, A., et al. 2019, MNRAS, 482, 5138
Bessell, M. S., & Brett, J. M. 1988, PASP, 100, 1134
Bessell, M. S., Castelli, F., & Plez, B. 1998, A&A, 333, 231
Blackwell, D. E., & Shallis, M. J. 1977, MNRAS, 180, 177
Blackwell, D. E., Shallis, M. J., & Selby, M. J. 1979, MNRAS, 188, 847
Blackwell, D. E., Petford, A. D., & Shallis, M. J. 1980, A&A, 82, 249
Casagrande, L., Ramírez, I., Meléndez, J., Bessell, M., & Asplund, M. 2010, A&A, 512, A54
Casagrande, L., Lin, J., Rains, A. D., et al. 2021, MNRAS, 507, 2684
Evans, D. W., Riello, M., De Angeli, F., et al. 2018, A&A, 616, A4
Fernley, J. A. 1989, MNRAS, 239, 905
Gaia Collaboration (Prusti, T., et al.) 2016, A&A, 595, A1
Gaia Collaboration (Babusiaux, et al) 2018, A&A, 616, A10
Gaia Collaboration (Brown, A. G. A., et al) 2021, A&A, 649, A1
González Hernández, J. I., & Bonifacio, P. 2009, A&A, 497, 497
Kurucz, R. L. 2005, Mem. Soc. Astron. Ital. Suppl., 8, 14
Lindegren, L., Hernández, J., Bombrun, A., et al. 2018, A&A, 616, A2
McCall, M. L. 2004, AJ, 128, 2144
Mucciarelli, A., & Bellazzini, M. 2020, Res. Notes Am. Astron. Soc., 4, 52
Mucciarelli, A., & Bonifacio, P. 2020, A&A, 640, A87
Ramírez, I., & Meléndez, J. 2005, ApJ, 626, 446
Riello, M., De Angeli, F., Evans, D. W., et al. 2021, A&A, 649, A3
Skrutskie, M. F., Cutri, R. M., Stiening, R., et al. 2006, AJ, 131, 1163
Stetson, P. B., Pancino, E., Zocchi, A., et al. 2019, MNRAS, 485, 3042
Yang, L., Yuan, H., Zhang, R., et al. 2021, ApJ, 908, L24

Appendix A: Colour-T_{eff} polynomial fits

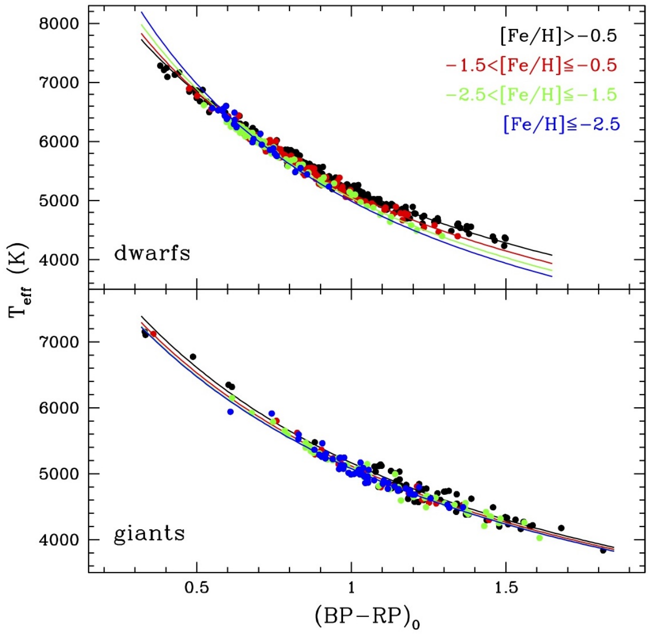

Fig. A.1. Behaviour of T_{eff} derived from IRFM by González Hernández & Bonifacio (2009) as a function of the $(BP-RP)_0$ colour for dwarf and giant stars (upper and lower panels, respectively). The stars are grouped according to their metallicity: [Fe/H]≤–2.5 dex (blue points),–2.5<[Fe/H]≤–1.5 (green points), –1.5<[Fe/H]≤–0.5 (red points), [Fe/H]>–0.5 dex (black points). The solid lines are the theoretical colour–T_{eff}relation calculated with [Fe/H]=–3.0 dex (blue line), –2.0 dex (red line), –1.0 dex (red line), +0.0 dex (black line).

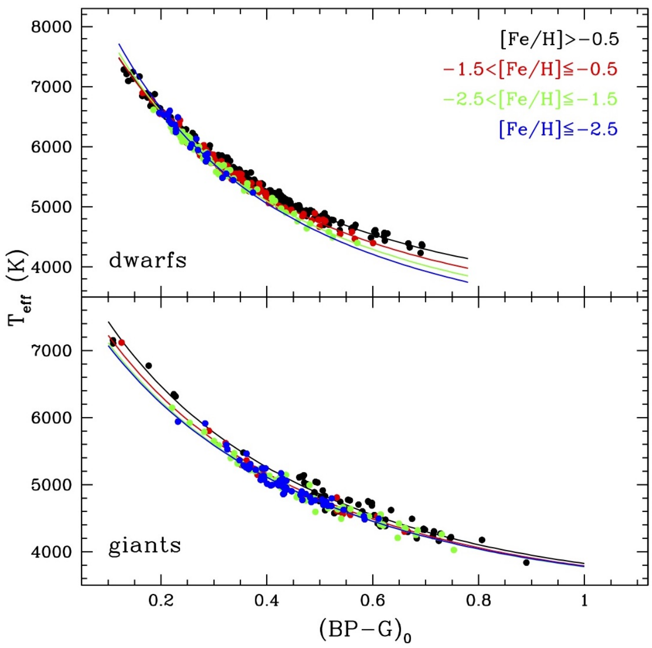

Fig. A.2. Same as Fig. A.1 but for the $(BP-G)_0$ colour.

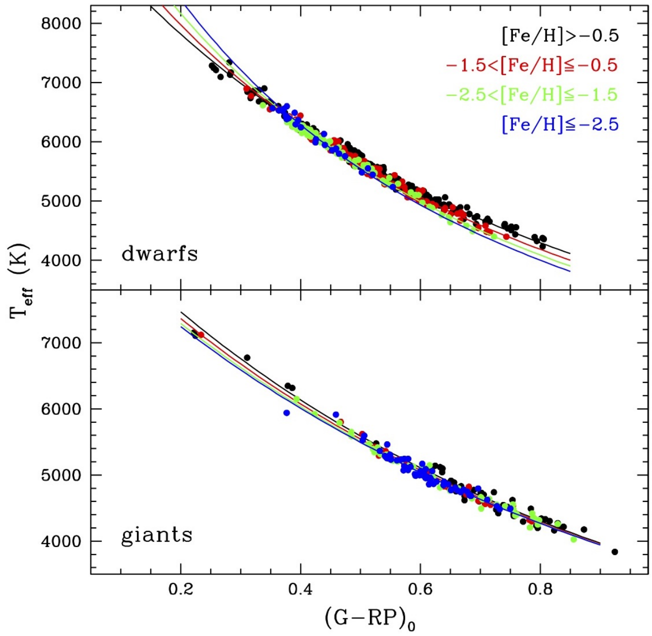

Fig. A.3. Same as Fig. A.1 but for the $(G-RP)_0$ colour.

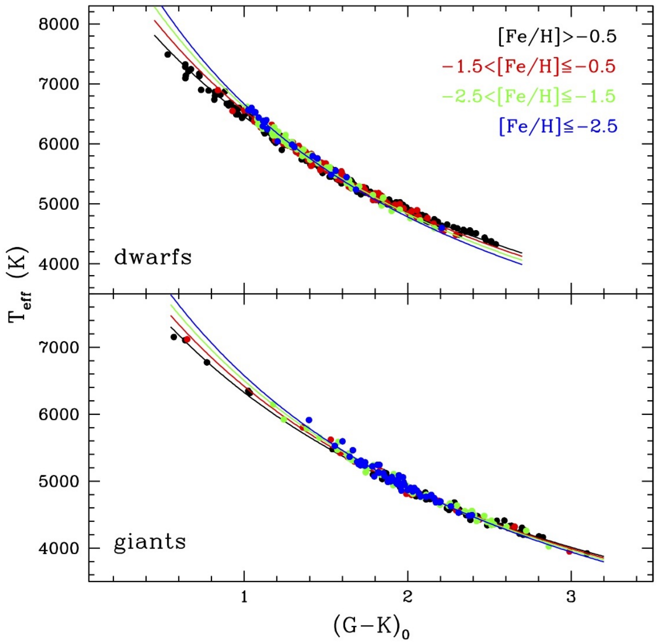

Fig. A.4. Same as Fig. A.1 but for the $(G-K_s)_0$ colour.

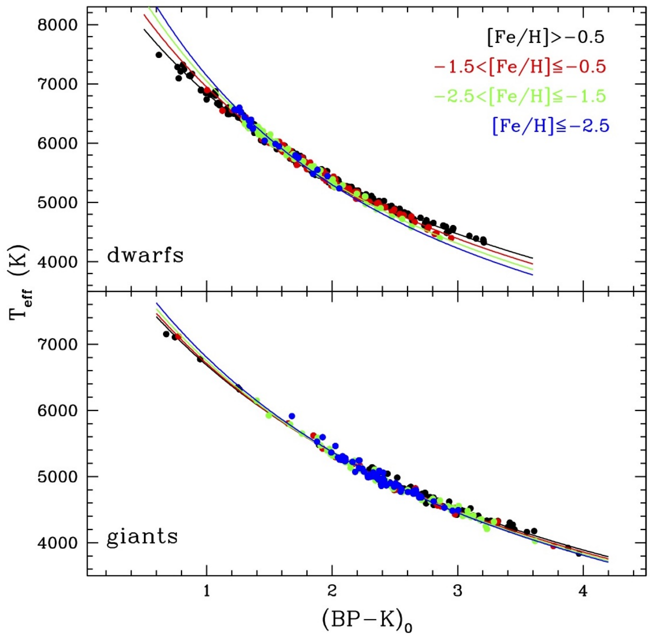

Fig. A.5. Same as Fig. A.1 but for the $(BP - K_s)_0$ colour.

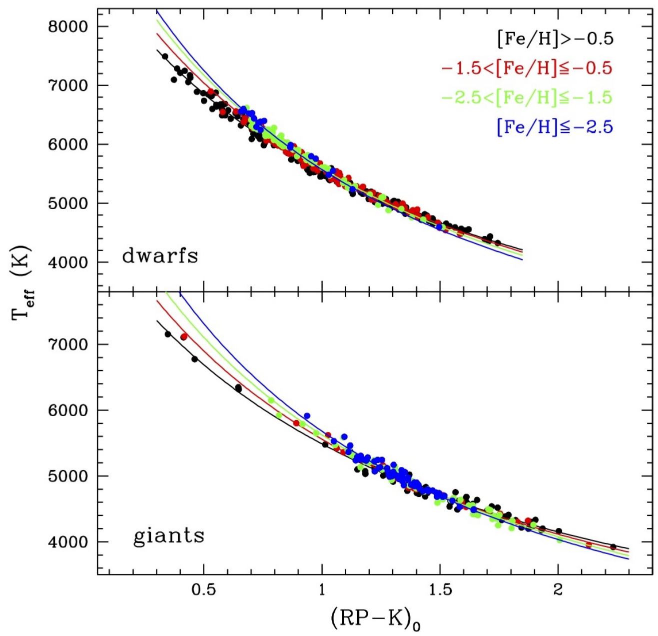

Fig. A.6. Same as Fig. A.1 but for the $(RP - K_s)_0$ colour.

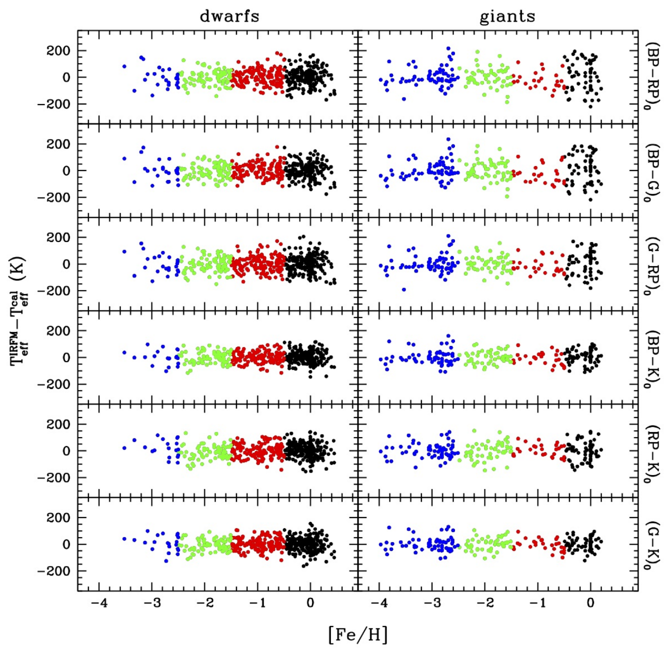

Fig. A.7. Behaviour of the temperature residuals as a function of [Fe/H] for all the colour–$T_{\rm eff}$ transformations discussed in this work. Colours are the same as in previous figures.

Appendix B: An alternative set of colour–$T_{\rm eff}$ transformations

As explained in Section 2, the usual approach to estimate the uncertainty in $T_{\rm eff}$ derived from colour–$T_{\rm eff}$ transformations is to propagate the colour error, sometimes adding in quadrature the 1σ dispersion of the fit residuals taken as a conservative estimate of the relation error. An appropriate propagation of the errors, including the uncertainties on the fit parameters and their possible covariance terms, is nevertheless provided in the following, by means of an alternative set of colour–$T_{\rm eff}$ transformations obtained with following fitting formula (reducing the off-diagonal terms of the covariance matrix):

$$\theta = c_0 + c_1C^* + c_2C^{*2} + c_3[{\rm Fe/H}]^* + c_4[{\rm Fe/H}]^{*2} + c_5[{\rm Fe/H}]^*C^*, \quad (B.1)$$

where C^* is the colour subtracted by the mean colour and $[{\rm Fe/H}]^*$ is the metallicity subtracted by the mean metallicity. Table 2 lists the coefficients c_i and the mean colour for each transformation (for all of them we assume −1.5 dex as mean metallicity). The 1σ dispersion and the number of used stars are the same listed in Table 1.

For a given pair of colour–metallicity, the relations 1 and B.1 (and the corresponding coefficients) *provide exactly the same results*. Relation 1 is more direct to use without needing to scale both colour and metallicity to the mean values used of the calibrators sample. It can be used when the 1σ dispersion of the fit is assumed as reliable estimate of the $T_{\rm eff}$ error due to the calibration itself. Relation B.1 needs the scaling of both colour and metallicity to the mean values used of the calibrators sample and should be used when the user is interested in calculating the $T_{\rm eff}$ uncertainty by propagating also the errors in the coefficients.

We list the normalised covariance matrix for each transformation. In each matrix, the raws and the columns correspond to the parameters c_0, c_1, c_2, c_3, c_4 and c_5, in this order.

– $(BP-RP)_0$ - *dwarf stars*

$$\begin{bmatrix} 1.000 & 0.045 & -0.229 & -0.034 & -0.503 & 0.075 \\ 0.008 & 1.000 & -0.288 & -0.414 & 0.359 & -0.699 \\ -0.021 & -0.288 & 1.000 & -0.012 & -0.114 & -0.198 \\ -0.035 & -0.414 & -0.012 & 1.000 & -0.615 & 0.350 \\ -0.583 & 0.359 & -0.114 & -0.615 & 1.000 & -0.400 \\ 0.017 & -0.699 & -0.198 & 0.350 & -0.400 & 1.000 \end{bmatrix}$$

– $(BP-RP)_0$ - *giant stars*

$$\begin{bmatrix} 1.000 & -0.070 & -0.335 & 0.001 & -0.651 & -0.013 \\ -0.024 & 1.000 & 0.110 & -0.281 & 0.056 & -0.387 \\ -0.050 & 0.110 & 1.000 & -0.342 & -0.124 & 0.108 \\ 0.003 & -0.281 & -0.342 & 1.000 & 0.281 & -0.050 \\ -1.252 & 0.056 & -0.124 & 0.281 & 1.000 & -0.279 \\ -0.005 & -0.387 & 0.108 & -0.050 & -0.279 & 1.000 \end{bmatrix}$$

– $(BP-G)_0$ - *dwarf stars*

$$\begin{bmatrix} 1.000 & -0.079 & -0.175 & 0.018 & -0.578 & 0.192 \\ -0.007 & 1.000 & -0.416 & -0.330 & 0.331 & -0.597 \\ -0.004 & -0.416 & 1.000 & 0.032 & -0.061 & -0.272 \\ 0.020 & -0.330 & 0.032 & 1.000 & -0.580 & 0.215 \\ -0.679 & 0.331 & -0.061 & -0.580 & 1.000 & -0.401 \\ 0.022 & -0.597 & -0.272 & 0.215 & -0.401 & 1.000 \end{bmatrix}$$

– $(BP-G)_0$ - *giant stars*

$$\begin{bmatrix} 1.000 & 0.068 & -0.340 & -0.067 & -0.638 & -0.046 \\ 0.012 & 1.000 & 0.222 & -0.432 & 0.039 & -0.391 \\ -0.014 & 0.222 & 1.000 & -0.293 & -0.081 & -0.018 \\ -0.115 & -0.432 & -0.293 & 1.000 & 0.193 & 0.223 \\ -1.238 & 0.039 & -0.081 & 0.193 & 1.000 & -0.301 \\ -0.010 & -0.391 & -0.018 & 0.223 & -0.301 & 1.000 \end{bmatrix}$$

– $(G-RP)_0$ - *dwarf stars*

$$\begin{bmatrix} 1.000 & 0.137 & -0.268 & -0.085 & -0.435 & -0.052 \\ 0.014 & 1.000 & -0.136 & -0.498 & 0.368 & -0.774 \\ -0.006 & -0.136 & 1.000 & -0.033 & -0.144 & -0.102 \\ -0.084 & -0.498 & -0.033 & 1.000 & -0.641 & 0.459 \\ -0.514 & 0.368 & -0.144 & -0.641 & 1.000 & -0.404 \\ -0.006 & -0.774 & -0.102 & 0.459 & -0.404 & 1.000 \end{bmatrix}$$

– $(G-RP)_0$ - *giant stars*

$$\begin{bmatrix} 1.000 & -0.226 & -0.345 & 0.060 & -0.630 & 0.019 \\ -0.038 & 1.000 & -0.001 & -0.074 & 0.077 & -0.400 \\ -0.012 & -0.001 & 1.000 & -0.434 & -0.161 & 0.238 \\ 0.100 & -0.074 & -0.434 & 1.000 & 0.354 & -0.349 \\ -1.263 & 0.077 & -0.161 & 0.354 & 1.000 & -0.256 \\ 0.004 & -0.400 & 0.238 & -0.349 & -0.256 & 1.000 \end{bmatrix}$$

– $(BP-K_s)_0$ - *dwarf stars*

$$\begin{bmatrix} 1.000 & 0.098 & -0.243 & -0.073 & -0.425 & -0.035 \\ 0.041 & 1.000 & -0.205 & -0.451 & 0.386 & -0.805 \\ -0.118 & -0.205 & 1.000 & -0.013 & -0.181 & -0.026 \\ -0.068 & -0.451 & -0.013 & 1.000 & -0.678 & 0.435 \\ -0.471 & 0.386 & -0.181 & -0.678 & 1.000 & -0.393 \\ -0.018 & -0.805 & -0.026 & 0.435 & -0.393 & 1.000 \end{bmatrix}$$

– $(BP-K_s)_0$ - *giant stars*

$$\begin{bmatrix} 1.000 & -0.021 & -0.313 & -0.038 & -0.680 & -0.064 \\ -0.015 & 1.000 & 0.135 & -0.278 & 0.037 & -0.499 \\ -0.246 & 0.135 & 1.000 & -0.358 & -0.111 & 0.133 \\ -0.067 & -0.278 & -0.358 & 1.000 & 0.262 & -0.001 \\ -1.327 & 0.037 & -0.111 & 0.262 & 1.000 & -0.206 \\ -0.055 & -0.499 & 0.133 & -0.001 & -0.206 & 1.000 \end{bmatrix}$$

– $(RP-K_s)_0$ - *dwarf stars*

$$\begin{bmatrix} 1.000 & -0.182 & -0.122 & 0.012 & -0.531 & 0.197 \\ -0.040 & 1.000 & -0.434 & -0.222 & 0.382 & -0.761 \\ -0.018 & -0.434 & 1.000 & -0.003 & -0.228 & 0.035 \\ 0.012 & -0.222 & -0.003 & 1.000 & -0.648 & 0.179 \\ -0.601 & 0.382 & -0.228 & -0.648 & 1.000 & -0.335 \\ 0.061 & -0.761 & 0.035 & 0.179 & -0.335 & 1.000 \end{bmatrix}$$

– $(RP-K_s)_0$ - *giant stars*

$$\begin{bmatrix} 1.000 & -0.021 & -0.315 & -0.033 & -0.688 & -0.081 \\ -0.008 & 1.000 & 0.176 & -0.271 & 0.054 & -0.512 \\ -0.077 & 0.176 & 1.000 & -0.346 & -0.094 & 0.169 \\ -0.060 & -0.271 & -0.346 & 1.000 & 0.226 & 0.054 \\ -1.353 & 0.054 & -0.094 & 0.226 & 1.000 & -0.176 \\ -0.038 & -0.512 & 0.169 & 0.054 & -0.176 & 1.000 \end{bmatrix}$$

– $(G-K_s)_0$ - *dwarf stars*

$$\begin{bmatrix} 1.000 & 0.166 & -0.225 & -0.111 & -0.407 & -0.116 \\ 0.056 & 1.000 & -0.102 & -0.457 & 0.328 & -0.823 \\ -0.068 & -0.102 & 1.000 & -0.028 & -0.206 & -0.018 \\ -0.105 & -0.457 & -0.028 & 1.000 & -0.663 & 0.448 \\ -0.468 & 0.328 & -0.206 & -0.663 & 1.000 & -0.341 \\ -0.050 & -0.823 & -0.018 & 0.448 & -0.341 & 1.000 \end{bmatrix}$$

– $(G-K_s)_0$ - *giant stars*

$$\begin{bmatrix} 1.000 & -0.057 & -0.323 & -0.013 & -0.680 & -0.072 \\ -0.031 & 1.000 & 0.136 & -0.220 & 0.035 & -0.502 \\ -0.147 & 0.136 & 1.000 & -0.383 & -0.114 & 0.200 \\ -0.023 & -0.220 & -0.383 & 1.000 & 0.277 & -0.070 \\ -1.344 & 0.035 & -0.114 & 0.277 & 1.000 & -0.175 \\ -0.046 & -0.502 & 0.200 & -0.070 & -0.175 & 1.000 \end{bmatrix}$$

Table B.1. Coefficients c_0,...,c_5 of the colour–T_{eff} relations (see Equation B.1) [a].

Colour	<Colour>	c_0	c_1	c_2	c_3	c_4	c_5
Dwarf stars							
$(BP-RP)_0$	0.8	0.8918	0.5120	-0.0353	-0.0065	-0.0020	-0.0395
		(0.0007)	(0.0041)	(0.0081)	(0.0007)	(0.0006)	(0.0032)
$(BP-G)_0$	0.3	0.8798	1.0774	-0.4677	-0.0065	-0.0031	-0.0752
		(0.0007)	(0.0084)	(0.0305)	(0.0007)	(0.0006)	(0.0064)
$(G-RP)_0$	0.5	0.9016	0.9905	0.2284	-0.0069	-0.0011	-0.0726
		(0.0008)	(0.0079)	(0.0330)	(0.0008)	(0.0007)	(0.0064)
$(BP-K_s)_0$	1.8	0.8977	0.2204	-0.0021	-0.0024	0.0005	-0.0158
		(0.0005)	(0.0013)	(0.0011)	(0.0006)	(0.0005)	(0.0010)
$(RP-K_s)_0$	0.9	0.8636	0.3824	-0.0121	0.0045	0.0029	-0.0220
		(0.0007)	(0.0030)	(0.0044)	(0.0006)	(0.0006)	(0.0021)
$(G-K_s)_0$	1.5	0.9015	0.2733	0.0016	0.0000	0.0015	-0.0163
		(0.0006)	(0.0018)	(0.0020)	(0.0006)	(0.0005)	(0.0014)
Giant stars							
$(BP-RP)_0$	1.1	1.0294	0.4031	-0.0344	-0.0059	-0.0020	-0.0009
		(0.0020)	(0.0059)	(0.0136)	(0.0012)	(0.0011)	(0.0050)
$(BP-G)_0$	0.5	1.0582	0.7372	-0.3710	-0.0085	-0.0039	0.0070
		(0.0021)	(0.0115)	(0.0507)	(0.0012)	(0.0011)	(0.0096)
$(G-RP)_0$	0.6	0.9962	0.8640	0.2347	-0.0046	-0.0012	0.0060
		(0.0018)	(0.0107)	(0.0511)	(0.0011)	(0.0009)	(0.0091)
$(BP-K_s)_0$	2.5	1.0338	0.1872	-0.0017	-0.0023	-0.0008	-0.0045
		(0.0012)	(0.0017)	(0.0015)	(0.0007)	(0.0006)	(0.0014)
$(RP-K_s)_0$	1.4	1.0382	0.3334	-0.0226	0.0016	0.0007	-0.0221
		(0.0015)	(0.0038)	(0.0061)	(0.0008)	(0.0008)	(0.0032)
$(G-K_s)_0$	2.0	1.0265	0.2429	-0.0035	0.0014	0.0007	-0.0089
		(0.0011)	(0.0021)	(0.0025)	(0.0006)	(0.0006)	(0.0018)

[a] For each relation the corresponding reference mean colour used for the fit is listed. The uncertainties for each coefficient are listed in brackets.